NERS 576 Final Report: On the Emission Spectrum of a Trapped Electron in a Relativistic Ion Bubble

Mike Johnson

Dec. 13, 2014

Abstract

In this paper, the trajectory of an electron trapped inside a uniform-density, spherical ion cavity is studied by analytical and numerical means. The intial analytical study establishes a qualitative model for electron motion, which is then reinforced by a case study via simulation. Finally, the results of this simulation are used to generate an estimate of the electron emission spectrum as a function of frequency. Although each portion of this analysis appears mathematically and physically consistent, the final result is several orders of magnitude above what is quoted in the literature.

1 Introduction

The high-energy physics community, in its quest to further the pursuit of science and industry, has a virtually limitless appetite for high-brightness, high-energy X-ray sources. Applications of such machines are numerous, ranging from imaging to fundamental physics. Yet in spite of this, the community is severly limited by the fact that synchrotrons, which are ponderously large and expensive to build and operate, remain the most viable way to produce such X-rays.

A rapidly developing alternative[1] to the synchrotron is the laser-driven plasma accelerator, which promises to shrink the size and cost of high-brightness, high-energy X-ray devices by orders of magnitude. This device generates a highly-relativistic bubble of ions which is then passed through a plasma. A portion of the electrons encountered by the ion bubble become trapped within it, thereafter undergoing extremely high-frequency oscillation as they rattle about inside the bubble. As these are charged particles undergoing periodic motion, the electrons then emit synchrotron radiation.

It is the goal of this paper to characterize this radiation's frequency dependence, as a step toward understanding how laser-driven plasma accelerators function. To this end, we will begin by developing a simple model of an ion cavity and a trapped electron (initially following [4] and [7] before branching off onto our own). After we have characterized our model, we will separate the electron's trajectory into an oscillatory and a non-oscillatory component, solving for each component analytically. However, the solutions so generated will not be sufficiently analytically tractible, so we will finally turn to numerics to generate an approximate emission spectrum for the electron for a test case. We will then compare our result to others published in the literature.

[1] See, for example, [3], [4], [5], and [7] among copious others.

2 Analytical Methods

2.1 Our Model

We will begin by assuming our ion cavity is spherical with radius r_b in the lab frame, constant-density with a plasma frequency of ω_p, non-evolving, and moving with a highly-relativistic Lorentz factor $\gamma_b \gg 1$. We will assume that the ion bubble is moving purely in the z-direction at a constant speed v_b; we will call the distance from the z-axis by r and the azimuthal angle by ϕ. Finally, we will assume there exists a sheath of electrons about the bubble that will cancel the electrostatic field from the ion cavity. We will interest ourselves in an electron that becomes trapped in such an ion bubble, which will produce electric and magnetic fields that are zero at its center and increase radially with distance from the center.

2.2 Field Equations

The fields experienced by our electron are then[2]

$$\mathbf{f}(z,r,t) = \begin{cases} -\frac{m_e\,\omega_p^2}{2}\left(\hat{z}\left(z(t) - v_b\,t - \beta_r(t)\,r(t)\right) + \hat{r}\left(1+\beta_z(t)\right)\frac{r(t)}{2}\right), & \text{inside bubble} \\ 0, & \text{outside bubble} \end{cases}$$

where $z(t)$, $r(t)$, etc. refer to the trapped electron, and $\beta_i(t) = \frac{v_i(t)}{c}$, so that boosting into the ion bubble's reference frame and normalizing units to m_e, ω_p, c, and $-e$ gives

$$\tilde{\mathbf{f}}(\tilde{z},\tilde{r},\tilde{t}) = \begin{cases} \frac{1}{2}\left(\hat{z}\;\frac{1}{\gamma_b}\left(\tilde{z}(\tilde{t}) - \gamma_b^2\,\tilde{v}_r(\tilde{t})\,\tilde{r}(\tilde{t})\right) + \hat{r}\left(1+\tilde{v}_z(\tilde{t})\right)\tilde{r}(\tilde{t})\right), & \text{inside} \\ 0, & \text{outside} \end{cases} \tag{1}$$

where the tildes indicate dimensionless variables.[3] The electron's equation of motion is thus

$$\frac{\mathrm{d}p_z}{\mathrm{d}t}(t) = \frac{1}{2\,\gamma_b}\left(\gamma_b^2\,v_r(t)\,r(t) - z(t)\right), \tag{2}$$

$$\frac{\mathrm{d}p_r}{\mathrm{d}t}(t) = -\frac{1}{2}\left(1+v_z(t)\right)r(t). \tag{3}$$

[2] See [7].

[3] These tildes will be omitted in the rest of the paper, but unless otherwise noted, all variables will be dimensionless.

Since we have assumed the ion bubble is highly relativistic, $\gamma_b \gg 1$, and so the first term in (2) dominates the second. Equations (2) and (3) then are

$$\frac{\mathrm{d}p_z}{\mathrm{d}t}(t) \approx \frac{\gamma_b}{2} v_r(t)\, r(t), \tag{4}$$

$$\frac{\mathrm{d}p_r}{\mathrm{d}t}(t) = -\frac{1}{2}\Big(1 + v_z(t)\Big)\, r(t). \tag{5}$$

The feedback implicit in equations (4) and (5) will create oscillating solutions, and the factor of γ_b in (4) will make these oscillations rapid. However, these fast oscillations will have little effect on the long-term trajectory of the electron, as the oscillations' contributions will largely cancel over a cycle. Instead, the long-term trajectory of the electron will be determined by the more gradual second term in (2). This long-term effect will look like

$$\frac{\mathrm{d}p_z}{\mathrm{d}t}(t) \approx -\frac{z(t)}{2\gamma_b}\,. \tag{6}$$

Thus we may divide the overall electron trajectory into a slow, "linear"[4] component and a fast oscillatory component:

$$\mathbf{v}(t) \approx \mathbf{v}^{\mathrm{osc}}(t) + \mathbf{v}^{\mathrm{lin}}(t),$$

where $|\mathbf{v}^{\mathrm{osc}}| \ll |\mathbf{v}^{\mathrm{lin}}|$ while $\left|\frac{\mathrm{d}\mathbf{v}^{\mathrm{osc}}}{\mathrm{d}t}\right| \gg \left|\frac{\mathrm{d}\mathbf{v}^{\mathrm{lin}}}{\mathrm{d}t}\right|$. It then follows that the Lorentz factor will have $\gamma\big(\mathbf{v}(t)\big) \approx \gamma\big(\mathbf{v}^{\mathrm{lin}}(t)\big)$, so that we can further assume $\gamma\big(\mathbf{v}^{\mathrm{lin}}(t)\big) \approx \gamma^{\mathrm{lin}} =$ (constant) over a single fast oscillation.

2.3 The Oscillatory Component

The oscillatory component of (4) and (5) is then

$$\frac{\mathrm{d}\mathbf{p}^{\mathrm{osc}}}{\mathrm{d}t}(t) \approx \gamma^{\mathrm{lin}} \frac{\mathrm{d}\mathbf{v}^{\mathrm{osc}}}{\mathrm{d}t}(t) = \hat{z}\ \frac{1}{2}\Big(\gamma_b\, v_r(t)\, r(t)\Big) - \hat{r}\ \frac{1}{2}\Big(1 + v_z(t)\Big)\, r(t).$$

This equation has solutions of the form

$$\mathbf{x}^{\mathrm{osc}} \approx \hat{z}\ \left(C_0\, t + C_1 + C_2\, \mathfrak{E}\Big(\mathfrak{F}^{-1}\Big(C_3\, t + C_4\,\Big|\, C_5\Big)\Big|C_5\Big)\right) + \hat{r}\ \left(C_6\, \mathfrak{Sn}\Big(C_3\, t + C_4\,\Big|\, C_5\Big)\right), \tag{7}$$

[4]The reason for calling it linear will become clear shortly.

where C_0, C_1, etc. are constants, $\mathfrak{E}(\phi\,|\,m)$ and $\mathfrak{F}(\phi\,|\,m)$ are the elliptic integrals of type E and F of argument ϕ and parameter m, and $\mathfrak{Sn}(\phi\,|\,m)$ is the Jacobi elliptic *sn*-function.[5] Although analyzing the z-component of (7) is not especially rewarding, the r-component is just a Jacobi *sn*-function. These are the elliptic equivalent of sine functions, and like them, *sn*-functions are periodic — the frequency of this one would be $k\,C_3$ for an elliptic constant k (analogous to $2\,\pi$). Unfortunately, the values of C_3 and k both depend on the starting positions and momenta of each of the components during the oscillation as well as γ^{lin}. Thus, although we can say that the r-component of (7) is periodic, determining its exact period is impossible for even a single oscillation, and furthermore, the "constants" in (7) depend on γ^{lin} and so are not really constant at all! Finally, we note that since the z-component of (7) has $p_z^{\text{osc}}(t) \sim \big(r^{\text{osc}}(t)\big)^2$, the z-component will have a similar frequency to the r-component, which will also be impossible to determine and also (slowly) varying from one oscillation to another.

2.4 The Linear Component

Turning to (6), then,

$$\frac{\mathrm{d}p_z^{\text{lin}}}{\mathrm{d}t}(t) \approx \frac{\mathrm{d}}{\mathrm{d}t}\left(\frac{v_z^{\text{lin}}}{\sqrt{1-\big(v_z^{\text{lin}}\big)^2}}\right) = -\,\frac{z^{\text{lin}}(t)}{2\,\gamma_b}\,.$$

Solutions to this equation satisfy

$$t = C + \sqrt{4\,\gamma_b\,(\gamma_0-1)+z_0^2}\;\mathfrak{E}\left(\sin^{-1}\left(\frac{z^{\text{lin}}(t)}{\sqrt{4\,\gamma_b(\gamma_0+1)+z_0^2}}\right)\;\middle|\;\frac{4\,\gamma_b(\gamma_0+1)+z_0^2}{4\,\gamma_b(\gamma_0-1)+z_0^2}\right)$$
$$-\,\frac{4\,\gamma_b}{\sqrt{4\,\gamma_b\,(\gamma_0-1)+z_0^2}}\;\mathfrak{F}\left(\sin^{-1}\left(\frac{z^{\text{lin}}(t)}{\sqrt{4\,\gamma_b(\gamma_0+1)+z_0^2}}\right)\;\middle|\;\frac{4\,\gamma_b(\gamma_0+1)+z_0^2}{4\,\gamma_b(\gamma_0-1)+z_0^2}\right), \tag{8}$$

where again C is a constant and $\mathfrak{E}(\phi\,|\,m)$ and $\mathfrak{F}(\phi\,|\,m)$ have the same meaning as previously. Since $z^{\text{lin}}(t)$ only appears inside an inverse sine function in (8), it must be that $z^{\text{lin}}(t) \sim \sin\big(f(t)\big)$ for some function $f(t)$. That is, for most commonly-encountered functions $f(t)$, $z^{\text{lin}}(t)$ will be periodic or will have something that "looks like" a period. However, as in the oscillatory case, determining exactly *what* the linear period is is not analytically feasible.

[5] See [1] for a description of elliptic integrals'/functions' properties.

2.5 Summary of Analytics

Having thus examined the problem analytically, we can only discuss a trapped electron's emission spectrum qualitatively, not quantitatively. We must now turn to numerical methods and analyze a representative case if we are to better understand the problem.

3 Numerical Methods

3.1 Our Test Case

To proceed, we will numerically integrate (2) and (3) with a fourth-order Runge-Kutta solver[6] for the case[7] of a bubble with $\gamma_b = 10$, $r_b = 10$ (in the lab frame), an initial momentum $\mathbf{p} = 0$, and an initial position $\mathbf{x} = -\hat{z}\,(0.95\,\gamma_b\,r_b) + \hat{r}\,(0.05\,r_b)$.[8,]

3.2 Graphical Numerical Results

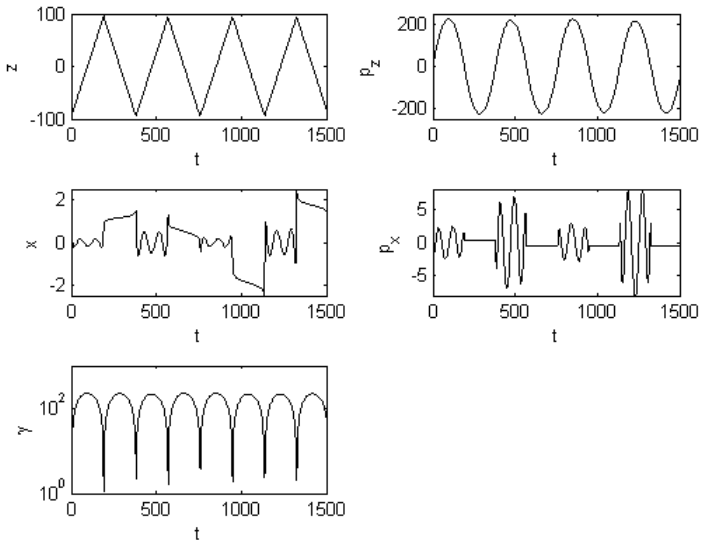

Fig. 1: The plots of $z(t)$, $p_z(t)$, $x(t)$, $p_x(t)$, and $\gamma(t)$ obtained via numerical integration of equations (2) and (3). Using x instead of r makes the plots more readable but does not alter physical quantities.

[6]The notes in [6] were exceedingly helpful here.

[7]The approximate magnitude of these parameters were taken from [7].

[8]These parameters were chosen to represent an electron that has just been (barely) trapped inside the bubble and that is only slightly off-axis.

In fig. 1[9], we see the output of this calculation. p_z has a sinusoidal shape for this case; because the amplitude of this sinusoid is much larger than 1 almost everywhere, $v_z \approx \pm c$ at almost all times, and so z has a sawtooth shape. On the other hand, p_r has a very different appearance: when $p_z > 0$, p_r oscillates roughly sinusoidally with a (very slowly) varying frequency, as predicted. However, when $p_z < 0$, p_r is constant and nearly zero. This is because a highly relativistic particle streaming parallel to a charged beam experiences electric and magnetic forces from the beam, but a highly relativistic particle streaming anti-parallel feels almost no forces.[10] Because $|p_r| \ll |p_z|$, $v_r \nsim c$, so the r plot does not have the sawtooth character of the z plot. Finally, we note that near the turning points of its trajectory, the electron has $\gamma \sim 1$, while away from the turning points, $\gamma \sim 100$. We are now in a position to use this information to determine what kind of radiation profile our simulated electron will emit.

3.3 Estimating an Electron's Emission Spectrum

The intensity of radiation as a function of frequency, $I(\omega)$, is given in [2] by

$$\frac{\mathrm{d}I}{\mathrm{d}\omega}(\omega) = \sqrt{3}\ \frac{e^2}{c}\ \gamma_{e,\,\mathrm{lab}}\,\frac{\omega}{\omega_c}\int_{\frac{\omega}{\omega_c}}^{\infty} K_{\frac{5}{3}}(y)\ \mathrm{d}y,$$
$$\omega_c \equiv \frac{3}{2}\ \gamma_{e,\,\mathrm{lab}}^3\,\frac{c}{R}\,, \tag{9}$$

where $K_{\frac{5}{3}}(x)$ is a modified Bessel function of type K and order $\frac{5}{3}$ and where R is a radius of curvature characterizing the electron's path. Equation (9) has physical units; normalizing it to the same scales as (1) yields[11]

$$\frac{\mathrm{d}\tilde{I}}{\mathrm{d}\tilde{\omega}}(\tilde{\omega}) = \sqrt{3}\ \gamma_{e,\,\mathrm{lab}}\,\frac{\tilde{\omega}}{\tilde{\omega}_c}\int_{\frac{\tilde{\omega}}{\tilde{\omega}_c}}^{\infty} K_{\frac{5}{3}}(y)\ \mathrm{d}y,$$
$$\tilde{\omega}_c = \frac{3}{2}\ \gamma_{e,\,\mathrm{lab}}^3\,\frac{1}{\tilde{R}}\,. \tag{10}$$

Since we are interested in the highest-intensity, highest-frequency component of the radiation emitted, we will pick electron parameters that maximize ω_c.

[9] Note that in our Runge-Kutta program, we refer to the variable x instead of r. This allows the non-axial component of position to become negative, which makes the plot of $r(t)$ much more readable. It does not change any of the physics — one can substitute $r(t)$ for $|x(t)|$ in the code and plots without effect.

[10] See chapter 2 of [8].

[11] Again, tildes will be dropped after this point and all quantities will be assumed dimensionless unless otherwise noted.

In that case, we will use the electron's properties at the center of the bubble, when $\gamma = \sqrt{1 + p_z^2 + p_r^2} \approx p_z \approx 220$ and $R \approx \frac{\gamma_b r_b}{2} = 50$. Since $\gamma_b = 10 \ll \gamma$ at the center of the bubble, we can then simply take $\gamma_{e,\,\mathrm{lab}} \approx \gamma \sim 220$. We then find

$$\frac{\mathrm{d}I}{\mathrm{d}\omega}(\omega) \approx 0.0012\,\omega \int_{\frac{\omega}{320000}}^{\infty} K_{\frac{5}{3}}(y)\,\mathrm{d}y. \tag{11}$$

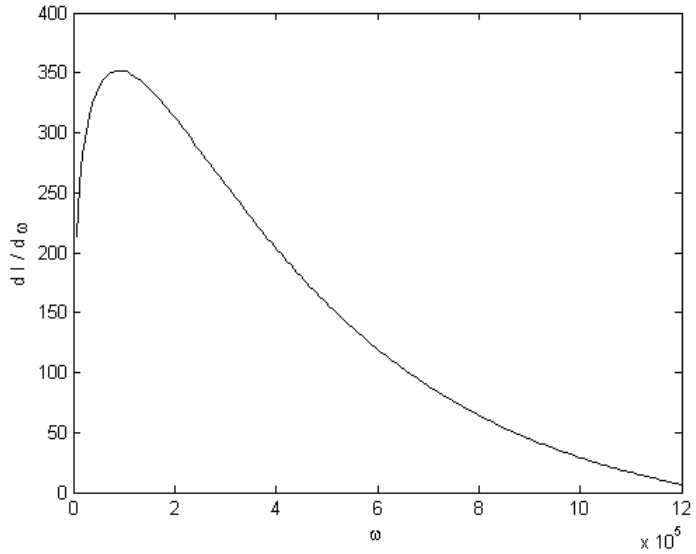

Fig. 2: The intensity of emitted radiation as a function of frequency.

Fig. 2 shows the result of numerically integrating (11). $\frac{\mathrm{d}I}{\mathrm{d}\omega}(\omega)$ has a maximum at $\omega = 9.0 \times 10^4$, so the frequency at which the electron will emit most brightly in this case will be (in physical units) $\omega \sim \tilde{\omega}\,\omega_p \sim 9.0 \times 10^4\,\omega_p$. For a plasma with a density of $n \sim 10^{24}\,\frac{\#}{m^3}$, this would give a peak intensity at $\sim 10^{16}$ Hz, which is many orders of magnitude away from anything reasonable![12]

4 Conclusion

Clearly our derivation has erred somewhere. It does not seem likely that the error is in our initial setup, as these same equations have been used to

[12] For example, [7] mentions frequencies of $\sim 10^{12}$ Hz.

good effect by several published authors. By the same token, our analytical work seems quite reasonable — it agrees qualitatively with previous published papers and with intuition. Our numerical solution to the electron's trajectory also fits with both our and others' work: the solution has all the expected properties and no surprises, which would not be the case if something were off by orders of magnitude. Finally, we turn to the spectrum estimate; the spectrum function itself is beyond reproach, as it comes from a well-respected textbook, so it seems most likely to this author that he has somehow misapplied this formula.

Regardless of this tripping at the finish line, this paper has presented several novel and noteworthy results in the analytical and numerical sections. It is the intent of the author to locate the remaining error and correct it as soon as possible, so that the preceding derivations can be properly tested and applied to the business of understanding the world.

References

[1] M. Abramowitz and I. Stegun. *Handbook of Mathematical Functions with Formulas, Graphs, and Mathematical Tables*. Dover Publications, 10th edition, 1972.

[2] J.D. Jackson. *Classical Electrodynamics*. John Wiley and Sons, Inc., 3rd edition, 1999.

[3] D.H. Bilderback, P. Elleaume, and E. Weckert. Review of third and next generation synchrotron light sources. *Journal of Physics B*, 38:773–797, 2005.

[4] I. Kostyukov, et al. Phenomenological theory of laser-plasma interaction in "bubble" regime. *Physics of Plasmas*, 11:5256–5264, 2004.

[5] S. Kneip, et al. Bright spatially coherent synchrotron x-rays from a table-top source. *nature: physics*, 6:980–983, 2010.

[6] W.H. Press, et al. *NUMERICAL RECIPES: The Art of Scientific Computing*. Cambridge University Press, 3rd edition, 2007.

[7] A.G.R. Thomas. Scalings for radiation from plasma bubbles. *Physics of Plasmas*, 17:1–12, 2010.

[8] H. Wiedemann. *Particle Accelerator Physics*. Springer-Verlag Berlin, 3rd edition, 2007.